Journal of Hydrology: Regional Studies 40 (2022) 101041

Contents lists available at ScienceDirect

Journal of Hydrology: Regional Studies

journal homepage: www.elsevier.com/locate/ejrh

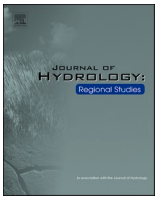

Recent water disposal and pore pressure evolution in the Delaware Mountain Group, Delaware Basin, Southeast New Mexico and West Texas, USA

Jun Ge [a,*], J.-P. Nicot [a], P.H. Hennings [a], K.M. Smye [a], S.A. Hosseini [a], R.S. Gao [a,b], C. L. Breton [a]

[a] Bureau of Economic Geology, Jackson School of Geosciences, The University of Texas at Austin, Austin, TX, USA
[b] Department of Geological Sciences, Jackson School of Geosciences, The University of Texas at Austin, Austin, TX, USA

ARTICLE INFO

Keywords:
Pore Pressure
Salt Water Disposal
Seismicity
Injection Well
Permian Basin

ABSTRACT

Study region: A flat, large, semi-arid plateau in the southwest United States (west Texas and southeast New Mexico) underlain by a deep Paleozoic sedimentary basin, the tectonic Delaware Basin, host of intensive hydrocarbon production.
Study focus: Impacts of injection of large volumes of water produced from oil and gas wells and injected through 1000 + disposal wells, in particular, pressure buildup, induced seismicity and their potential consequences, in a formation underlying fresh-water aquifers but separated from them by thick layers of evaporites. The target formation is the Delaware Mountain Group (DMG) of Permian age and consisting of up to 4500 ft (~1400 m) of mostly fine-grained, deepwater siliciclastic slope and basin deposits (sandstones, siltstones, and minor limestones). A flow model was developed and calibrated from well log data, stratigraphic data, petrophysical analyses, and core data (123 ×170 mi^2 - 1 ×1 mi^2 grid size) complemented with dynamic injectivity information based on surface injection pressures and rates of the disposal wells.
New hydrological insights for the region: Injection of 5.8 billion barrels (0.92 billion m^3) of waste water has generated regional pressure increases in the DMG mostly in the 100–400 psi (0.7–2.8 MPa) range: (1) creating strong artesian conditions that, combined with the presence of numerous historical boreholes, could connect DMG and fresh-water aquifers; and (2) generating conditions leading to actually observed moderate induced seismicity.

1. Introduction

The Permian Basin of west Texas and southeast New Mexico (Fig. 1 and Fig. S1) is an important oil-producing basin in the southwest region of the USA whose production had been declining until the mid-2000 s, but that has seen a strong recovery related to development of unconventional resources. Unconventional resources include very low-permeability rocks, such as shales, that are typically the source of hydrocarbon accumulations in conventional reservoirs. Their development was made possible by the concurrent advances in horizontal drilling technology (1–3 km of horizontal section) and hydraulic fracturing stimulation, during which large amounts of water are injected to fracture the rock and increase its permeability (Nicot et al., 2014; Vidic et al., 2013; Nicot and

* Corresponding author.
E-mail address: jun.ge@beg.utexas.edu (J. Ge).

https://doi.org/10.1016/j.ejrh.2022.101041
Received 28 August 2021; Received in revised form 18 December 2021; Accepted 16 February 2022
Available online 23 February 2022

Scanlon, 2012). However, a well-known consequence of unconventional production in the Delaware Basin (DB), a sub-basin of the Permian Basin, is a high water-oil ratio, amounting to produced water volumes multiple times that of the oil produced (Scanlon et al., 2017, 2020b; Lemons et al., 2019); perhaps the highest of any shale play in the USA. The produced water volume is also multiple times that of fluids used for hydraulic fracturing but some of it can be reused for fracturing unconventional formations (Saini and Mezei, 2016). The Permian-age Delaware Mountain Group (DMG) is the major target for produced water disposal. The first fully documented salt water disposal (SWD) well was drilled in the early 1980 s. However, since then, many more SWD wells have been drilled to service the increased waste disposal needs of a growing oil and gas industry that has increased production from unconventional reservoirs underlying the DMG, and that has raised concerns about induced seismicity, disposal capacity, and pressure increases. Historically, the

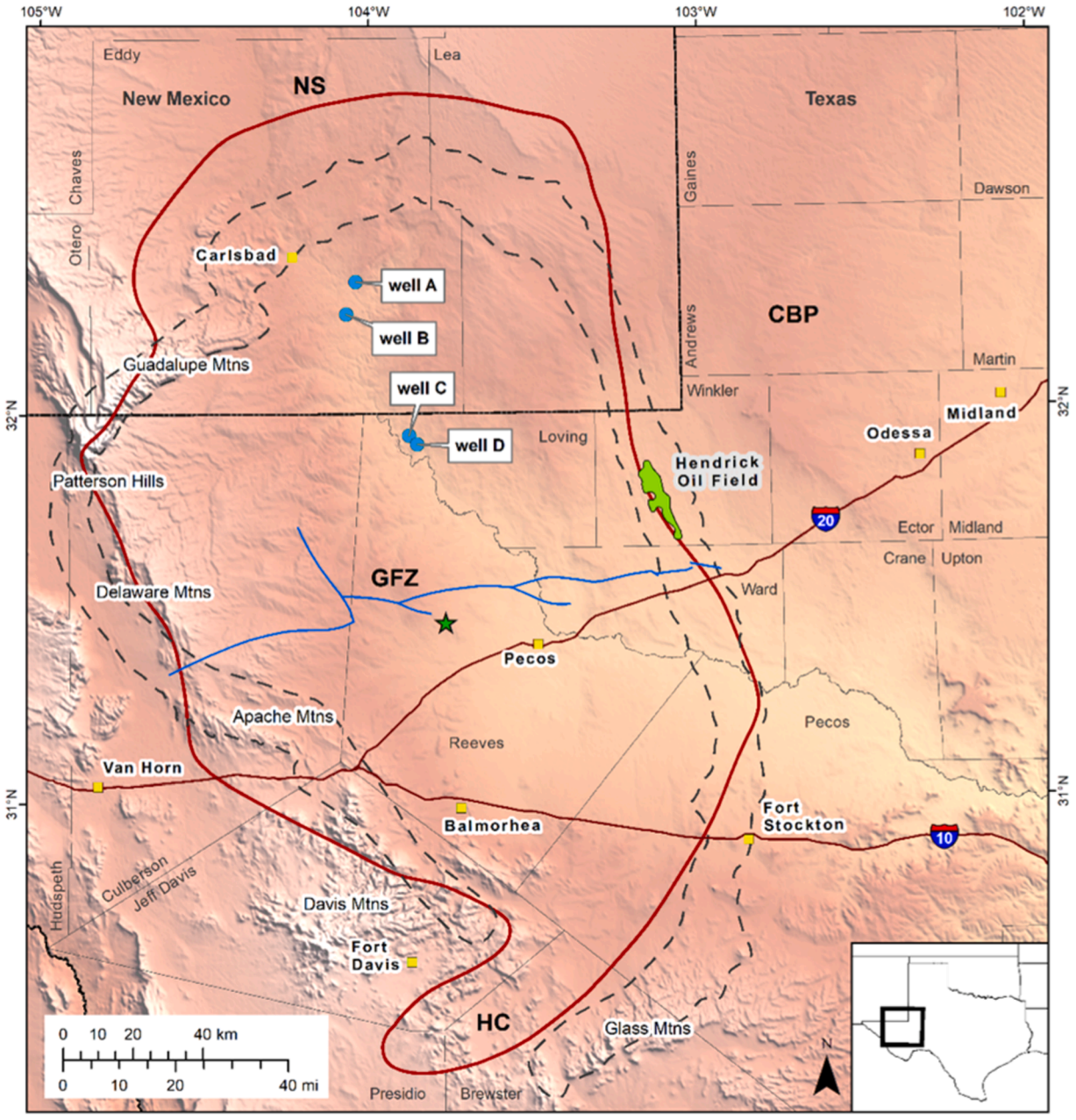

Fig. 1. Location map of the study area with topographic, geographic, and geological features. Approximate boundaries of the tectonic Delaware Basin outlined by solid red line. Footprint of the Capitan Reef outlined by dotted black line. The yellow squares are towns. The Grisham fault zone delineated by solid blue line. Footprint of a large Hendrick oil field (historical significance) shown in green. Data from wells A to D were used in the model calibration. GFZ = Grisham Fault Zone; HC = Hovey Channel; CBP = Central Basin Platform; NS = Northern Shelf. The green star represents the location of the type log well in Fig. 2.

disposal of waste fluids and seismicity have been shown to be related (Healy et al., 1968), and, more recently, in basins across the south-central USA (Barnes and Halihan, 2019; Hennings et al., 2019; Skoumal et al., 2018, 2019; Langenbruch and Zoback, 2016). The volume of water injected in the DMG (a total of 5.8 billion barrels as of December 2019) has been at a historical maximum in recent years (Fig. S2), and exceeds the cumulative volume of fluids injected in other nearby seismic-prone areas such as the Fort Worth Basin (2.23 billion barrels) (Gao et al., 2021), but is less than the amount injected in Oklahoma (11.5 billion barrels) (Scanlon et al., 2020b). The regional pressure increase can potentially impact the overlying and adjacent aquifers, including strings of desert springs such as in the Balmorhea, Texas area (Uliana et al., 2007; Robertson et al., 2019), through ~60,000 oil and gas production wells (HIS, 2017–, 2020), many of which have been abandoned for more than half-a-century. It can favor anthropogenic dissolution of the overlying evaporites, and, in extreme cases, lead to the formation of sinkholes such as observed in the Wink Sink, Winkler County, in the Hendrick oilfield (Fig. 1) (Kim et al., 2019; Paine et al., 2009).

The objective of this study is to provide estimations of pore pressure evolution in the DB for use in causal assessment and mitigation of induced seismicity (Dvory and Zoback, 2021; Morris et al., 2021; Savvaidis et al., 2020), and for management of the DMG as an injection disposal resource in the DB, including risk assessments. As the need for protecting fresh water resources intensifies, there is growing interest in understanding proximal water-bearing formations underlying fresh-water aquifers (Bloomfield et al., 2020; Kang et al., 2019). We developed a numerical flow model focusing on the pore pressure history of the DMG main injection intervals (from 1983 to 2019). The modeling approach is very straightforward in principle and relies on the direct application of Darcy's law in a single-phase flow system although the study is concerned with water injection rather than withdrawal. The detailed stratigraphy of the modeled formations allowed the development of a conceptual model for flow parameters somewhat balancing data scarcity. In addition, we introduce the concept of using injection pressure and injection rate (whose ratio is injectivity or specific capacity) as a means to develop the model permeability field. Because of the lack of wells dedicated to pressure and head monitoring, we instead use injection pressure at the ground surface to calibrate the regional model. The long-term sustainability of such a large regional injection scheme has been raised and some operators are turning to water recycling or beneficial use after treatment instead of injection as a means to dispose of the produced water (Scanlon et al., 2020a).

2. Geological background

2.1. Geological setting

Covering an area of ~10,000 mi^2 (25,000 km^2), with surface elevations ranging from ~3000–4500 + ft amsl (~1000–1400 + m amsl), the DB is a sub-basin of the Permian Basin province of west Texas and southeast New Mexico. The DB and its flanks have been affected by several extensional and contractional tectonic events cumulatively leading to the present day tectonic fabric (Horne et al., 2021 and references therein). Paleozoic sediments rest on a Proterozoic basement and the oldest sediments in what would become the DB are mostly carbonate platform deposits of Ordovician to Devonian age (Fig. S3). The thickness of Paleozoic sediments to the Pennsylvanian varies around ~8000 ft (2400 m) and the basin fill is more than 20,000 ft (>6 km) thick at its deepest (Fig. S4). The surface topography of the DB is a flat plateau with moderate topography in the west (Guadalupe and Delaware Mountains) and south (Apache and Davis Mountains), and a slope dipping gently to the east and southeast. Subsidence in the DB was most active during the early Permian. The thick Permian-age strata are named, in order of decreasing age: Wolfcampian, Leonardian, Guadalupian, and Ochoan (Fig. S3). The cumulative thickness of the Permian deposits can be as high as 15,000 ft (4500 m) in the main depocenters, but less than half of that thickness along some of its margins.

The DB was quiescent during most of the Mesozoic but some minor Triassic-age lacustrine deposits (Dockum) and clastic and carbonate sediments related to the Cretaceous transgression (Western Interior Seaway) are preserved. Much of these more recent sediments have been eroded owing to the Neogene tilting of the Texas Craton, which includes the DB, that exposed the western margin of the Permian Basin (Brown, 2019; Anon, 2019). Cenozoic alluvium (Pecos Valley Alluvium), locally very thick, is derived from prior salt dissolution and related subsidence, and these sediments are capped by aeolian deposits.

The main structural features of the DB were in place by the end of the Permian with (1) reverse upwardly attenuating thrust faults with NNW-SSE strike on the DB's eastern margin separating it from the Central Basin Platform (CBP); (2) development during the Guadalupian and coeval of the DMG deposition of an important reefal system ringing most of the DB, the Capitan Reef complex, whose core is made of massive carbonates; and (3) an E-W structural feature, variously called the Mid-Basin High, Grisham Arch or Grisham Fault Zone, south of Loving County that displaces all formations older than the Leonardian Bone Spring Formation (Van Der Loop, 2017). Basement-rooted faults, often with large throws, die-out upward into the Wolfcamp before they reach the DMG (Horne et al., 2021). Two important tectonic events occurred in the Cenozoic; (1) regional uplift during the Laramide orogeny (~60 Ma) and (2) tilting due to Basin and Range tectonics (10–20 Ma) (Sinclair, 2007). These two events did not fundamentally change the structure of the DB but altered the dynamics of fluid flow within it. Note that, although the CBP was exposed and its carbonates underwent multiple episodes of karstification and erosion during the Permian, the DB basinal sediments of Permian age were not exposed until these Cenozoic events.

2.2. The Permian Period and Delaware Mountain Group

Permian deposits, all marine in origin, are coarser clastics (with infrequent depositional carbonates) transitioning from the mudstone-rich facies in the Wolfcamp Formation to the clastic- and carbonate-rich Leonardian Bone Spring Formation, to the mostly silty and sandy Guadalupian DMG, and capped by thick Ochoan evaporitic deposits, mostly anhydrite of the Castile Formation and

mostly halite of the Salado Formation (Fig. S3). The Wolfcamp Formation lies conformably on Pennsylvanian shales and consists mostly of silica-rich mudstones. The Wolfcamp Formation represents the primary interval currently targeted by oil and gas operators. Bone Spring sediments conformably overlie Wolfcamp sediments and consist of alternating siliciclastic intervals, also often targeted by operators, and more carbonate-rich intervals. Because the Bone Spring Formation was deposited in a more quiescent basin already filled with sediments, its thickness is more uniform across the DB with an estimated average thickness of ~3000 ft (~900 m).

DMG sediments represent the unconformable continuation of the Bone Spring sedimentation with much less abundant carbonates, and consist mostly of initially clay-poor arkosic to subarkosic siltstones and fine sandstones with minor detrital carbonates (Dutton, 2008; Nance, 2020a; Smye et al., 2021). The transition to the DMG at the top of the Bone Spring Formation is marked by fine-grained intervals (carbonate mass transport deposits with increasing organic-rich siltstones), collectively named the Cutoff Shale; one of them, the Avalon Shale, is targeted by operators in New Mexico (Hurd et al., 2018; Carr, 2019; Smye et al., 2021). The DMG is traditionally divided into three units (increasing overall permeability), and, in ascending stratigraphic order, are the Brushy Canyon, Cherry Canyon and Bell Canyon Formations. The DMG cumulative thickness can be up to 4500 ft (~1400 m) in the DB mid-section, but decreases to < 2000 ft (<600 m) at its northern and southern edges. The sediment deposition mechanisms have been described as lowstand turbidity currents transporting and distributing siliciclastic sediments from the platforms to the DB in fan complexes and as debris flows of carbonates taken from the exposed platforms or outer-shelf back reef deposits (Smye et al., 2021; Nance, 2020a). The abundant, sometimes organic-rich siltstones, are interpreted as starved, transgressive to highstand, eolian or suspension deposits (Smye et al., 2021; Nance, 2020a; Dutton et al., 2005). Numerous sea-level fluctuations generated the interspersed nature of siltstones and sandstones.

Proximal deposits are channelized whereas distal deposits are more sheet-like with a low degree of amalgamation or sand-on-sand contact (Zhang et al., 2017) as stratigraphically distinct successions of highstand sands are disconnected by intervening lowstand siltstones suggesting unfavorable vertical connectivity (Smye et al., 2021). Examination of net sand maps shows a clockwise rotation of the main fairway trends from the northern margin (NS channels of the Brushy Canyon) to the eastern margin (NS and EW channels in the Cherry canyon and NE-SW channels in the Bell Canyon, in which formation they extend far into the DB) (Smye et al., 2021; Nance, 2020a). Net sand volumes average 46%, 68% and 70% for the Brushy Canyon, Cherry Canyon, and Bell Canyon, respectively, but carbonate dominates on the DB margins (Smye et al., 2021). The Brushy Canyon has been described as containing coarser sandstones but, because of a lack of sorting and of post-deposition diagenesis, its porosity and permeability are lower overall than that the finer, but better sorted overlying formations. Carbonate units are rare in the Brushy Canyon but become abundant upwards, with more extensive and laterally continuous intervals in the Bell Canyon, compartmentalizing the formation horizontally. Some, such as the Lamar Limestone Member at the top of the Bell Canyon, and the Manzanita Member at the top of the Brushy Canyon, can be traced basin-wide (King, 1948; Hampton, 1989). The DMG formations were partly exhumed during regional tilting in the Neogene and crop out in the Delaware Mountains to the west of the DB on an along-strike length of ~50 miles (80 km). The DMG is impacted by many shallow normal faults with small throws that delineate small grabens (Staniewicz et al., 2020; Charzynski et al., 2019). These faults are not believed to have a significant impact on regional flow.

The overall prograding Capitan Reef complex marks the transition between basinal and shelf sediments, almost completely encircles the DB, and is approximately coeval of the Bell Canyon (Fig. S5). The eastern arm of the Reef, along the CBP, is mostly buried except to the south of the DB where it crops out in the Glass Mountains. To the north, crossing into New Mexico, the Capitan Reef is shallow and host of a fresh water aquifer and then emerges in the Guadalupe Mountains as the main surface expression of the western arm of the Reef (Standen et al., 2009; Hiss, 1976). The large late Cretaceous fault that uplifted the Guadalupe Mountains ("Border Fault") during the Laramide Orogeny, dropped the remainder of the western arm deep into the subsurface (except locally in the Patterson Hills and Apache Mountains) until it disappears across from the Glass Mountains, completing the horseshoe shape of the reef complex and leaving open the channel linking the DB to the open ocean. The backreef debris toward the platform and the shelf sediments are generally described as fractured and of good permeability whereas the carbonate debris of the forereef are understood as more compact and of lower permeability (Nance, 2020a).

The Castile Formation is restricted to the DB proper, but younger formations of the Ochoan series (Salado, Rustler and Dewey Lake Formations) extend outside of it. The anhydrite of the Castile has a sharp but conformable transition with the top of the Bell Canyon Formation. It has a basal limestone towards the margins of the DB. Interbedded halite is frequent in the Castile. The salt from the Salado Formation (halite with frequent sylvite and other complex evaporite minerals) is the thickest in Lea County in New Mexico and along the eastern side of the DB but is barely present in the western half of the DB due to active dissolution by meteoric water. It has also been considerably thinned along the footprint of the Capitan Reef on the eastern margins of the DB, allowing for the deposition of the thick Cenozoic Pecos Valley Alluvium.

2.3. *Hydrogeology and oil and gas production*

Several studies have investigated the general features of groundwater flow in the DMG under natural conditions. Others studies have been narrowly focused on producing reservoirs (Dutton et al., 2005). Although the Wolfcamp Formation and part of the Bone Spring Formation and of the underlying Pennsylvanian Formation have been described as strongly overpressured (Rittenhouse et al., 2017; Bryndzia et al., 2019), strata younger than Guadalupian, including the DMG and Capitan Reef, are normally pressured, but some sections can be under artesian conditions (Knowles and Lang, 1947; Hiss, 1976, 1980). Uplift and tilting had an important impact on regional hydrogeological flow in the DB. Flow in all normally pressured formations is currently towards the south and east, driven by the general topographic slope of the Permian Basin (Nicot, 2021). The tilting initiated the flow of water that had been nearly static or flowed slowly in a flat terrane for millions of years (e.g., Ferguson et al., 2018). This tectonic activity promoted recharge in units

exposed along the western edge of the DB (e.g., Lee and Williams, 2000). The western margin of the DB can be recharged through the fractured Capitan Reef and the DMG outcrop as evidenced by low TDS formation water. Natural secular flow in the DMG is generally described as very slow, and directed towards the east and southeast (Hiss, 1980; Sharp, 2001). The salinity of the DMG is highly variable from fresh to hypersaline but spatially structured (see later sections for full discussion). Salinity from oil fields can reach up to ~250,000 ppm (West Texas Geological Society WTGS, 1982). Historical papers and reports with data on the DMG (McNeal, 1965; TWDB Texas Water Development Board, 1972; Zaengle, 1995) show large spatial contrasts in TDS, with lower TDS in the western side of the DB, increasing to high values adjacent the CBP, and reverting to low values on the Guadalupian carbonates of the CBP.

Aquifers with fresh to brackish water are present in the Ochoan Rustler and Dewey Lake Formations. and also include the Triassic Dockum Aquifer, the Cretaceous Edwards-Trinity Aquifer and the Cenozoic Pecos Valley Aquifer, as well as the Guadalupian Capitan Reef. Depending on their locations and access to the end users, all these aquifers are used as water source by oil and gas operators and is the carrier fluid for hydraulic fracturing stimulations. The Capitan Reef Aquifer and DMG are in direct contact with each other. The hydrodynamic nature and degree of interconnectivity at the margins of Permian Basin is an important consideration for modeling pore pressure.

The northern section of the Capitan Reef is an important aquifer for the City of Carlsbad and Eddy County in New Mexico, the Capitan Aquifer, (Fig. 1), and is recharged in the Guadalupe Mountains where the ancient reef crops out. The eastern arm of Capitan Reef is well hydraulically connected to the shelf deposits through permeable backreef sediments, but connection is intermittent with the basinal deposits because of the low permeability of the forereef sediments. For example, the large Hendrick oil field in Winkler County, located on the CBP (Fig. 1) produces low TDS water and has been shown to be hydraulically connected to the Capitan Reef (Hiss, 1976). Hiss (1976) noted a slight decrease in the potentiometric surface of DMG wells between 1920 and 1970. He hypothesized that oil and water production from reservoirs on the CBP and northern shelf hydraulically connected with the Capitan Reef caused the pressure decrease. Large produced water volumes ultimately withdrawn indirectly from the Capitan Aquifer were compounded by large volumes of water directly withdrawn from it for waterflooding purposes up to the 1960 s. Overall withdrawals were large enough to reverse flow directions in the Capitan Aquifer with a current pressure deficit centered on Winkler County (Hiss, 1976; Sharp, 2001; Uliana, 2001). This strong pressure signal was apparently detected in historical DMG potentiometric measurements (Hiss, 1976). This would suggest hydraulic communication and potential attenuation of excess pressure in the DMG if it bled into the Capitan Reef. However, many wells in the Capitan Reef on the eastern arm are in recovery mode (Jones, 2014) with increasing water levels that cannot be discerned from pressure bleeding related to water injection in the DMG. An examination of recent water level measurements in a limited number of Capitan Reef water wells with acceptable time series (28 wells) do not show a recent change in their long-term trends, but these measurements do not necessarily suggest there are not potential active exchanges.

Historical (conventional) oil and gas production targeted mostly DMG sandstone reservoirs, starting in the 1920 s, with associated forays into Bone Spring, Pennsylvanian, Devonian, and Ellenburger reservoirs since the 1980 s (a total of ~9000 wells have been drilled, with ~ 4000 are still active, Fig. S6 and Fig. S7). Wells were principally located along the eastern and northern margins of the DB (Nance, 2020a) with the greatest production coming from wells in the Bell Canyon (Dutton et al., 2003), then the Cherry Canyon and lastly the Brushy Canyon. Annual oil production from the DMG increased steadily from the 1950 s to late 2010 s with a peak of 20 + million barrels in 2015 (cumulative production of 600 + million barrels). Cumulative production in the DMG using conventional methods was estimated to be ~350 million barrels in the early 2000 s, at the onset of the shale revolution in the DB (Dutton et al., 2005; Potter et al., 2020), that is, cumulative oil production of 250 + million barrels in the DMG occurs in parallel to injection activities. In the 2010 s, along with the development of the underlying reservoirs in the Wolfcamp and Bone Spring Formations, operators added low-permeability organic-rich self-sourced siltstones to their targets, which contributed significantly to the 2015 production peak (EIA, 2020). Wolfcamp and Bone Spring unconventional development provides most of the current production in the DB (10,000 + hydraulically fractured wells). A significant consequence of DB unconventional operations is the high water-oil ratio, as high as 3 vol/vol (Nicot et al., 2020; Scanlon et al., 2017). These volumes are much higher than in the neighboring Midland Basin and many other unconventional plays. This produced water represents a significant technical and economic challenge to the industry as it now faces increased induced seismicity (Frohlich et al., 2020; Schultz et al., 2020), potential overpressure, and diminishing storage capacity (Scanlon et al., 2020b; Gogri et al., 2018). The very low permeability of the producing formations does not favor reinjection of the produced water. Instead, the bulk of produced water from unconventionals is injected into DMG formations. The cumulative saltwater volume disposed into more than 1000 DMG SWD wells reached > 5.6 billion barrels by December 2019.

Water production from conventional DMG reservoirs (3.4 billion barrels to date) follows the typical model of increasing water cut (fraction of water in the produced fluids) as production matures with most of the water being reinjected into the reservoir for pressure maintenance. It follows that overall pressure changes are only due to hydrocarbon production and that this short-path water cycle can be neglected. An important caveat relates to ~400 DMG wells that can be considered unconventional and have produced 0.42 billion barrels of water by December 2019, which are counted in the 5.8 billion barrels of water injected into DMG formations through SWD wells. Most of these wells are in Lea and Eddy counties in New Mexico.

Most of the sand-hosted DMG reservoirs are described as oil reservoirs with no gas cap at discovery and having a relatively quickly exhausted solution gas drive (Galloway et al., 1983; Dutton et al., 2005; Nance, 2020a), suggesting poor connection to the surrounding aquifer and, potentially, some pore space with depleted pressures. This was confirmed by sharp pressure drops over the local areas surrounding oil fields (Hiss, 1976). There is no recent measurement available to assess the degree of pressure recovery after production has ceased. Nance (2020a) stated that oil recovery efficiency is < 15% in most reservoirs even with secondary recovery because of the complex geometry of the reservoir and of the lack of a sustained driving mechanism. In general, slope and basin systems, such as the DMG, host reservoirs with the poorest sweep efficiency. Some reservoirs underwent successful tertiary recovery CO_2 floods (Potter et al., 2020) although the overall recovery efficiency remained low. Ford Geraldine field, which produced > 30 million barrels from

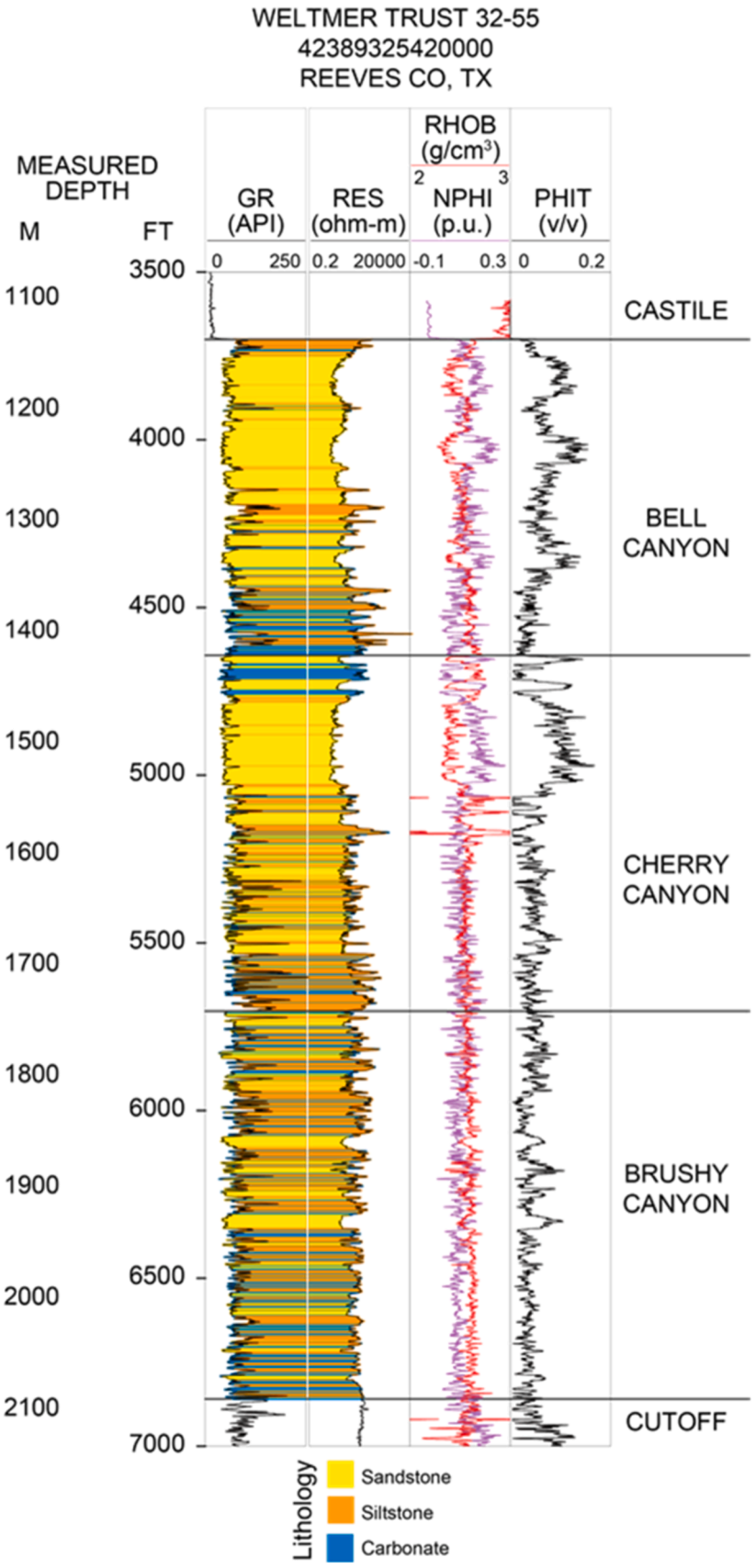

(caption on next page)

Fig. 2. Representative petrophysical log of the DMG for Weltmer Trust 32–55, located in Reeves County, TX. The log shows the dominant lithology of the Bell, Cherry and Brushy Canyon Formations as interpreted from gamma ray (GR, Track 1) and resistivity (RES, Track 2) log cutoffs. Raw bulk density (RHOB) and neutron porosity (NPHI) logs are shown in Track 3, and porosity (PHIT) as interpreted from a multi-mineral petrophysical model is shown in Track 4. The location of this type log well is shown by the green star in Fig. 1.

the upper part of the Bell Canyon, is the largest DMG field in the DB with an original oil in place of ~100 million barrels (Dutton et al., 1998). Fields close to the CBP, and along the eastern boundary of the DB, are described as having a water drive, likely related to the nearby Capitan Reef. The fact that very few oil reservoirs are known to be present in the Capitan Reef (Nance, 2020b) does not negate water exchanges between the Capitan Reef and DMG, as two-phase flow dynamics dictates that flow of the non-wetting phase (oil) can be impeded while that of the wetting phase (water) is not.

3. Data source summary

The construction of the flow model is a three-step process. Step 1 is the development of the quality-controlled database of injection well data as described below. In specific support of this research, Smye et al. (2021) provide Step 2 – the DMG reservoir description, which was used to construct a geocellular model. The geocellular model has the stratigraphic structure of the model through correlation of geophysical logs for 1090 wells (HIS, 2017–, 2020) distributed across the DB (Fig. 2). Porosity values were also extracted from a subset of the same dataset (327 wells). In Step 3, porosity values were upscaled in the geocellular model and implemented in the flow model proper to populate the grids. SWD well monthly injection volumes and average wellhead pressures were obtained from the state oil and gas regulatory agency, the Railroad Commission of Texas (RRC), H-10 forms, and from Enerdeq IHS Markit. The data were quality-controlled building on previous experience (Gao et al., 2021; Lemons et al., 2017). Note that, because operators report well operation data only once a year, there is a lag of about 15 months until this information can be considered complete. In addition, RRC provided 23 files with bottom hole pressure (BHP) and step rate test results. The BHP information is used to confirm the initial pressure gradient in the model.

Permeability data were also collected from historical publications on individual oil reservoirs (over 80 fields in DMG) and from the analysis of this data, from which a porosity-permeability transform was derived (Smye et al., 2021; Dutton et al., 2005). Additional data were taken from recently drilled RRC SWD permit files; a total of 15 step-rate tests were used to estimate permeability. Physical characteristics of the SWD wells, such as perforated intervals, open hole or cased status, and tubing dimensions were sourced from Enerdeq IHS Markit.

Compressibilities were estimated from the data in literature guided by RRC data. Temperature data were extracted from measured downhole values (HIS, 2017–, 2020). Salinity data was obtained from public domain sources: (1) USGS Produced Waters Database (Blondes et al., 2018) containing ~350 DMG historical samples (mostly collected in the 1960 s and 1970 s) along the margins of the DB and (2) New Mexico Water and Infrastructure Data System (Cather et al., 2016) which recently disseminated a snapshot of produced water geochemistry from 2014 to 15 (~650 DMG samples) as well as recent data points from Nicot et al. (2020). Oil and gas production history, production well locations, and target intervals were extracted from HIS, . (, 2017–, 2020)

4. Model construction and methods

4.1. Model structure

The area of interest covers the entirety of the DB and the model targets the DMG and Capitan Reef formations. It includes whole or parts of eight counties in west Texas and two counties (Lea and Eddy) in southeast New Mexico (Fig. 1). The areal extent is constrained by the structural boundaries of the DB: Capitan Reef complex to the east and to the north and DMG outcrop to the west. All side boundaries are assumed no-flow, which is a suitable assumption for a model of this large extent and the nature of the boundaries. Most of the injection occurs in the eastern half of the DB, not far from the high permeability Capitan Reef, whose proximity could buffer the model pressure variations in that area, and that is akin to the traditional approach of modeling water drive reservoirs (e.g., van Everdingen-Hurst model). The impacts of the Capitan Reef are analyzed in the Sensitivity Analysis section. No faults are in the model even though they exist in the DMG (Hennings et al., 2021a,2021b and 2021b), but many are minor with small throws compared to the thickness of the modeled units and of uncertain properties. They are not believed to have caused significant offsets of the model layers or to limit transverse flow because of the general absence of clay minerals that might reduce across-fault transmissibility (Ortiz et al., 2019). However, anecdotal information operators suggest transmissive flow parallel to the fault planes. Anisotropy possibly created by fault-parallel permeability enhancement is not studied here but this work is important input to more advanced analysis.

The top of the model domain is the top of the Bell Canyon Formation or, equivalently, the bottom of the Castile Formation The bottom of the model domain is the bottom of the Brushy Canyon Formation or, equivalently, the top of the Bone Spring Formation (Cutoff Shale). For the purpose of this model, top and bottom boundaries are assumed to be no flow because of the significant contrast in matrix permeability. Geochemical observations of water of clear meteoric origin on the western side of the DB, show that recharge has occurred in the recent past, and could be currently occurring; however, the recharge rate is too low to play a role for the short timeframe considered in this model. No study of recharge to the DMG exists but an overlying aquifer with a similar footprint and outcrop located in the same general area (Rustler Aquifer) has been attributed a recharge of 3 mm/year or less (Ewing et al., 2012).

For the purpose of establishing the layering for the flow model, the geocellular model was constructed using the Petrel software

(v.2019.4) (Schlumberger, 2019). A total of 1090 wells were used to correlate formation tops over the ~20,000 mi^2 of the study area (Smye et al., 2021). The three DMG formations (Bell Canyon, Cherry Canyon, and Brushy Canyon) were identified through these correlated tops. Formation thicknesses vary from the edge to the center of the DB and they also pinch out completely at some locations. Three lithologies (sandstone, siltstone, and carbonate) were defined in the model.

The Computer Modelling Group's (CMG) modeling package CMG-STARS, v.2019.10. (Computer Modeling Group CMG, 2019) was used to simulate pore pressure history. The code computes fluid properties such as viscosity and density as a function of temperature, pressure, and salinity. The model output is pressure rather than head because of the variable salinity, and therefore of the variable water density (e.g., Langevin and Guo, 2006). The model has 18 layers for the three DMG formations. Each formation is arbitrarily split into 6 layers of equivalent thickness in order to accommodate many short perforated SWD intervals, as well as 12 layers for the Capitan Reef. The corner-point grid is 123 × 170 mi^2 (198 ×274 km^2) with 123 × 170 × 30 cells of approximately 1 × 1 mi^2 (1.6 ×1.6 km^2) and includes 215,621 active cells. The average cell thickness is 163 ft (50 m) and the thickness of 85% the cells around the median ranges from 70 to 278 ft (21–85 m). Grid cells are aligned in the y direction with one of the main structural directions (NNW-SSE) that makes the eastern boundary with the CBP. Perpendicular structure (x direction) is the high permeability channels of the Bell Canyon and Cherry Canyon and, which is also aligned with the smaller faults.

4.2. Property distribution

The porosity and permeability fields (Fig. 3 and Fig. S8) were constructed in the Petrel software. A total of 334 wells with relevant petrophysical logs were used to model the porosity field through geostatistical analysis and sequential gaussian simulation. Permeability values were obtained through a more elaborate workflow making use of the measured porosity the injectivity of SWD wells.

The porosity values from log interpretation range from 10% to 25% for sandstones, from 5% to 10% for siltstones, and are less than 5% for carbonates (Smye et al., 2021). Well log data (~0.5 ft or ~15 cm vertical resolution) were upscaled in the geocellular model and extended across the entire layer through geostatistical and sequential gaussian simulation modeling (spherical model with a small nugget effect; low variance, and ~2–10 miles (3.2 −16 km) range). Overall, lithologies can be continuous over long distances at the regional scale (siltstone drapes, carbonate members, channel sandstones), which suggests a large geostatistical range, at least before upscaling, but also can be variable at the local scale, which suggests a high nugget effect. We opted to keep a relatively small nugget effect to avoid convergence problems when some of the hundreds of injection wells, about which little is known, are located in a randomly assigned low permeability cell. Porosity values estimated from well logs show differences with respect to the three DMG formations. Average porosity by formation are shown in Table S1, with a global average of 9%. Most cells were assigned a porosity between 3% and 15%, but locally, porosity can be > 20%. The mean porosity of Bell Canyon and Cherry Canyon Formation is higher than that of the Brushy Canyon Formation.

There are two contributions to the permeability field: 1) the porosity-permeability transform based on the log-derived porosity and core analysis, and 2) the estimated injectivity-derived permeability from available flowing well head pressure and flow rate history from SWD wells (Fig. S9). Note that there is no overlap between the two well sets. A porosity-permeability transform was developed with more than 9000 data points (Smye et al., 2021). It was observed that the relationship persists across variations in texture and facies. The porosity-permeability relationship can be used as a "permeability index". The permeability field upscaled from the "index" values was complemented by larger-scale permeability values estimated from injection rate and SWD well head pressure (from 594 out of 1008 wells) and step-rate tests obtained from the RRC.

The second dataset of injectivity-derived permeability lacks the vertical resolution provided by the petrophysical study, but reflects the field permeability that best accommodates the injection rate. The injectivity-derived permeability was estimated by assuming steady-state flow conditions, constant water viscosity of 1 centipoise (1 kPa•s), constant effective radius of 1000 ft (304.8 m), and wellbore radius of 0.25 ft (0.076 m). These permeability values were added to the model at control points (SWD wells), accounting that SWD well locations are biased towards higher permeability zones. The use of injectivity or specific capacity is not uncommon in developing flow models of regional aquifers (e.g., Nicot et al., 2013) but is typically used to complement results from more traditional pump tests in areas with a lack of well data. In this study, the approach is applied to the entire model using high-volume injection wells.

The final uncalibrated permeability field was then generated by co-kriging with the porosity field. Average permeability by formation varies within a limited range and overall average permeability is ~18 md (1000 md or 1D corresponds to a hydraulic conductivity of 0.86 m/day). Typical values range from 0.4 to 200 md for > 99% of the cells, with very few cells > 1D. Overall, permeability values in the Bell Canyon and Cherry Canyon Formations are higher than that in Brushy Canyon Formation (Table S1). However, the base case model does not assume horizontal permeability anisotropy.

Little vertical communication at the regional scale was assumed in the base case, with vertical permeability 10% of the horizontal permeability. The rationale is two-fold: 1) the presence of extensive low-permeability carbonate layers at the regional scale between the Brushy Canyon and Cherry Canyon and between the Cherry Canyon and the Bell Canyon; and 2) the strong stratification of the sediments at the bed level as well as the poor degree of amalgamation at various scales (Smye et al., 2021; Dutton et al., 1998). Given the magnitude of pore pressure modeled, it is likely that injection will cause hydraulic fracturing near wells with a high injection rate which would increase vertical communication. These results can be used to address this phenomenon.

Base case pore compressibility of the rock formations in the DMG, a component of the storage coefficient, was calculated to be 7.5×10^{-6} psi^{-1} (1.09 GPa^{-1}) (Dutton et al., 1998, Ford-Geraldine field). Based on a 9% average porosity, this value is consistent with other studies (e.g., 5.12 $\times 10^{-6}$ psi^{-1} or 0.74 GPa^{-1} from Hall (1953); 9.79×10^{-6} psi^{-1} or 1.42 GPa^{-1} from Newman (1973). The salinity distribution is discussed in the Initial Conditions section.

4.3. Fluid budget

The DB has a long history of oil and gas production, both from DMG conventional and unconventional reservoirs and from underlying unconventional reservoirs (mainly Bone Spring and Wolfcamp Formations). Most produced water from conventional reservoirs was reinjected into the same formations for pressure maintenance or waterflooding (Lemons et al., 2019). In this study, we assumed that conventional water production and injection cancelled each other at the spatiotemporal scale of the model, and they are not further considered, although an unknown amount of produced water may have been pumped into "evaporation" pits before the 1950 s. However, water production through DMG unconventional wells amounts to 0.42 billion barrels and must be accounted for in the model. A total of 1071 SWD wells within the modeled area have injected ~5.8 billion barrels of water from January 1983 to December 2019, the last month with complete data for analysis. Typical injection rates range from 1000 to 8000 barrel/day, with high-rate wells injecting more than 60,000 barrel/day into the Bell Canyon Formation. Some wells have low average injection rates < 300 barrel/day. Most perforations of the SWD wells are completed in the Bell Canyon Formation, followed by the Cherry Canyon Formation, and fewer wells still in the Brushy Canyon Formation.

Cumulative oil production from the DMG is ~0.6 billion barrels at surface conditions with no associated gas and this volume is large enough to be included in the flow model. The oil density from most DMG fields is generally 38–42°API gravity (West Texas Geological Society WTGS, 1982). Using 39°API (Nance, 2020a), and assuming solution gas is methane and the initial gas oil ratio is ~4000 ft^3/barrel at standard conditions (HIS, 2017–, 2020), the equivalent reservoir volume of 1 barrel oil produced at the surface is ~1.6 barrel in the subsurface. Oil production was assigned to the cells corresponding to the field location and depth.

Approximately 1.9 trillion cubic feet (Tcf) at standard conditions of (mostly solution) gas have been produced from the DMG conventional reservoirs (HIS, 2017–, 2020). Although some free gas could be released during production, accumulate in a newly created gas cap, and affect the bulk compressibility and the pressure in the formations, there is no evidence of such phenomenon. On the contrary, solution gas seems to be exhausted quickly, and the affected area is small compared to the much larger basin size model, therefore the impacts would negligible to the overall pressure evolution in the DMG formations in its entirety.

4.4. Initial conditions

Initial conditions of pressure and temperature were estimated using an analysis of initial shut-in pressure measurements obtained from drill-stem tests. The pressure was distributed in the model cells by assuming hydrostatic conditions with a pressure reference point located in the cell with the highest elevation, which is a cell close to the outcrop area. The initial pressure gradient is 0.49 psi/ft (11.08 kPa/m) (Fig. S10 and Table S2) and model initial pressure values range from 174 to 4050 psi (1.2–27.9 MPa).

Geothermal gradient varies with depth. We adopted an averaged geothermal gradient of 1.25°F/100 ft (22.75 °C/km) (Fig. S10 and

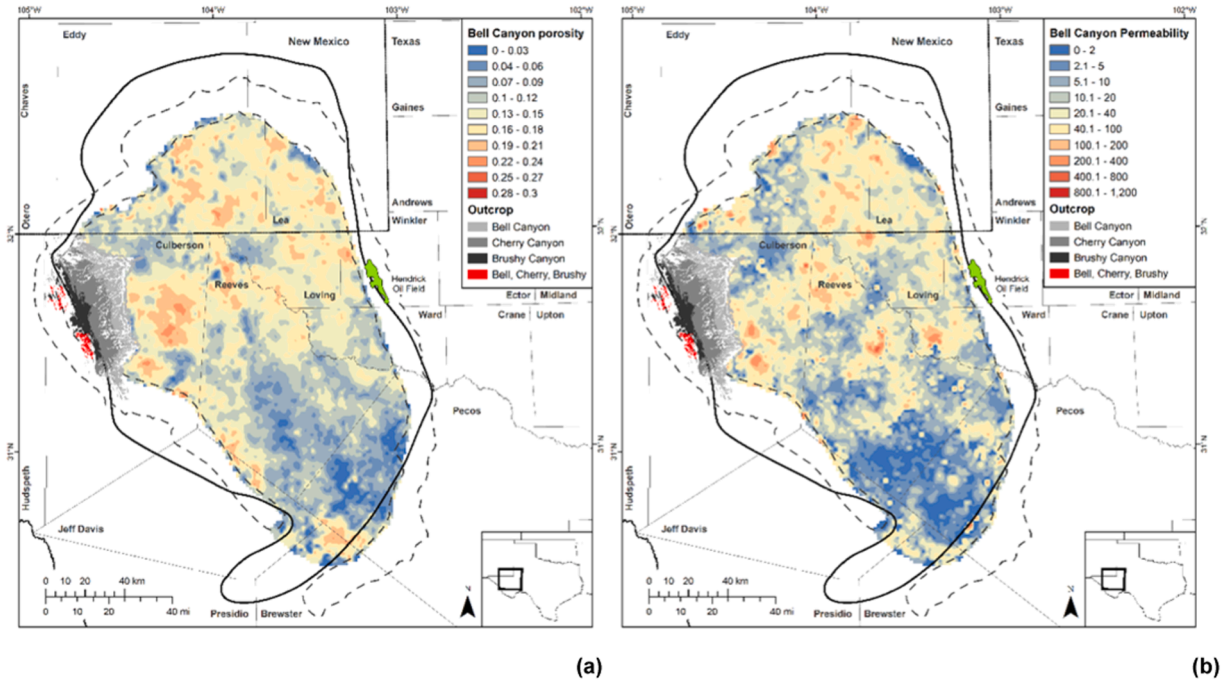

Fig. 3. (a) Porosity (volume fraction) and (b) permeability (md) for the top layer of the Bell Canyon Formation. Properties for the other two formations are shown in the Supplementary Information (Fig. S8). Note the DMG outcrops on the western side of the basin and the geometric progression of the permeability scale.

Table S2) with a constant surface temperature of 64°F (17.8 °C). The temperature in the model ranges from 64°F (17.8 °C) to ~167°F (75 °C). The injected water can be assumed at the temperature of 64°F (17.8 °C), but is immediately set at thermal equilibrium with the resident water of the cell it is injected into. The non-isothermal mode of the software is not utilized. All gridblocks stay at the same temperature imposed by their depth. Temperature values vary cell by cell and impact the fluid properties (density, viscosity, compressibility), but not the rock properties (compressibility, porosity, permeability).

The DMG exhibits a large TDS range, varying from fresh to brackish on the western margins of the DB next to where the DMG crops out and the aquifer is recharged. This phenomenon is confirmed by meteoric water invasion, from the west and north, following the general tilt of the region) to extremely saline at > 300 g/L in the east-central part of the basin center (Nicot et al., 2020). However, many of the historical salinity samples have a poor depth resolution. The close proximity of the overlying Castile and Salado Formations would suggest that halite dissolution is the source of the high salinity in the DMG and that the upper sections of the DMG should have a high TDS value, potentially suggesting regional convective instabilities. However, if several samples clearly show halite and anhydrite dissolution, geochemical arguments strongly suggest that many high salinity samples stem from Ochoan evaporative brines (Nicot et al., 2020), supporting the assumption of a density-stratified system (Hiss, 1976). We conclude that the salinity distribution correlates approximately with depth, and because more accurate data is lacking, we derive a linear function to represent salinity variations with depth. Water is modeled as a mixture of two geochemical components, saline water of 900 ppm at the shallowest depth and saline water of 250,000 ppm at the deepest part of the model. Initial salinity field is modeled as containing variable fractions of these 2 components.

The unconventional plays in the Permian Basin produce water with a TDS ranging from < 20,000 ppm to > 200,000 ppm (Nicot et al., 2020). Therefore, we used a constant injection water salinity of 60,000 ppm, which is close to the statistical mode of the data and tested values ranging from 20,000 ppm to 150,000 ppm in the sensitivity analysis. Gridblock salinity values evolve over time and are controlled by the injection and related flow.

4.5. Model calibration

The actual DMG flow system is in a transient state at a geological time scale as modified Permian-age evaporative brines are being slowly purged and replaced by meteoric water, which, in some places, is saturated with dissolved halite (Nicot et al., 2020). However, for the purpose of this model, we considered the system to be at equilibrium prior to injection (no flow and density-stratified). Because of the subsurface complexity, which includes various feedback loops (e.g., salinity on density and viscosity), the initial "at equilibrium" pressure field (with a maximum pressure change <0.5 psi over a period of 100 years) is reached by running a long model transient before SWD injection starts. During the long transient phase, the system is considered open to reach full hydrostatic conditions given the initial pressure, temperature and salinity conditions.

Calibration of the model is done over the entire model, and relies analyzing available surface wellhead injection pressures and convert them into BHPs. The wellhead flowing pressures range from ~0 psi to > 3500 psi (0 to >24.1 MPa) with an average of 1250 psi (8.6 MPa). The BHPs were derived using an algorithm by considering head and friction loses (0–2725 psi or 0–18.8 MPa, respectively) that are estimated by assuming the absolute roughness coefficient of 1.3×10^{-5} in (2.74×10^{-5} m) for the steel well casing (Bourgoyne et al., 1986). The estimated BHP values range from ~850 to ~6200 psi (~6.0 to ~42.8 MPa).

Not all reported wellhead injection pressure data can be directly used in the model because many are clearly inaccurate measurements. A typical example is where constant high pressures are recorded for several years despite varying injection rates. Such anomalous data typically represent maximum permitted pressure, not actual injection pressure. Very detailed and accurate, but confidential, operator data suggest a strong correlation between wellhead pressure and rate. In addition, several mechanisms visible on the injection history of individual wells, such as change in permeability following a workover, are not reflected in the model. To account for wellhead injection pressure data globally, each dataset was evaluated and assigned a confidence rating, with 0 for inaccurate data, 0.6 for general consistency with injection rate to 1 for cases with sequences of data with pressure being very consistent with injection rate. The inaccurate data are subsequently removed from inclusion in the model. The accepted pressure data were converted to estimated BHPs and compared to the modeled BHPs at the same injection wells. There is a total of > 15,000 useful data points over time and space (taken from 569 out of 1071 available SWD wells) (Fig. S11).

4.6. Sensitivity study

A sensitivity analysis was performed to evaluate parameters known to impact pressure behavior. Each parameter was varied individually without including cross-correlation effects (Table S3). For each simulation case, the long transient was run for the system to reach equilibrium before the start of injection. Porosity, horizontal and vertical permeability, horizontal permeability anisotropy, compressibility, temperature gradient, formation and injection water salinity are varied within a reasonable range from the base case values. In addition, scenarios related to the base case conceptual model were also evaluated when there was oil production, oil and water production, and the Capitan Reef gridblocks were inactive. In the base case, and for most of the sensitivity runs, no water is produced. However, a scenario must be considered where some of the water produced from DMG oil and gas reservoirs is disposed in SWD wells along with water produced from the underlying unconventional plays rather than reinjected close by for pressure maintenance or waterflooding (and thus ignored in the model). Such is the case for unconventional DMG wells. If water is locally reinjected after production, the local water cycling has no impact on regional pressures and does not need to be modeled. Whereas, if injected into SWD wells, this water (~1.5 billion barrels) needs to be accounted for in the model by being produced with the oil and then injected.

Results of the sensitivity analysis are evaluated using two metrics: (1) an illustrative value of the difference in pressure (ΔP)

between start of injection and last time step; rather than the median or average of the entire model, impacted by the large number of cells with no pressure changes, we use a more robust metric, a measure of the maximum pressure increase. However, rather than using the absolute largest value of all cells, the 99th percentile of the cells sorted in increasing ΔP is chosen in order to avoid outlier effects; and (2) the misfit (root mean square error) value computed as the sum of the square differences between estimated BHPs and model results at selected injection wells and at the same monthly time period normalized by the number of data points.

5. Results

Results are presented as maps of pressure deviations (ΔP) from the initial state (Fig. 4), focusing on the top layers representing the DMG: Bell Canyon, Cherry Canyon, and Brushy Canyon Formations. The Bell Canyon and Cherry Canyon Formations have the higher porosity and permeability distribution, and therefore have attracted the bulk of field operations and injected water. The higher permeability also leads to larger plume sizes, but with smaller pressure buildup. The Bell Canyon Formation includes more well-sorted sandstones and more consistently oriented sandstone channels that extend further into the DB. The channels have higher porosity and permeability, and higher amalgamation ratio (~connectivity), but are somewhat thinner with a median thickness of ~900 ft (270 m), as opposed to that of the Brushy Canyon and Cherry Canyon Formations at ~1000 ft (330 m) for both. Simulation results show pressure buildups ranging mostly from 100 to 400 psi (0.69–2.76 MPa), and locally exceeding 500 psi (3.45 MPa) near some injection sites (Fig. 4 and Fig. S12). High pressure buildups have become more common in recent years due to a dramatic increase in injection volumes. The lateral extent of pressure plumes is larger in the Bell Canyon and Cherry Canyon Formations, consistent with the larger volumes of water being injected as these formations have a higher storage capacity (Smye et al., 2021). Analyses of estimated BHP values and corresponding modeled pressures indicates that most calibration points fall along or close to the 1:1 line that denotes the best fit to the data (Fig. S13 and Fig. S14). History matching done for a few wells (Fig. 5) also show a good match between the modeled BHPs and the BHPs estimated from the field data (calculated RMSE for those wells range from 100 to 250 psi).

The sensitivity analysis shows that the pressure increase is sensitive to horizontal permeability and compressibility, the two parameters controlling pressure diffusion (Fig. 6 and Fig. S15, Table S3). The horizontal permeability field controls pressure buildup, which determines both on plume size and the maximum increase. A multiplier of 5x applied uniformly to the permeability field will cause a ~30–60% decrease in the pressure buildup, whereas a multiplier of 0.2x will lead to an equivalent pressure increase. The second most important parameter is compressibility. Doubling or halving the compressibility of the rock will result in a ~30–35% change in pressure buildup. The anisotropy of horizontal permeability in either direction will increase pressure differentials by ~10%. The effects from porosity, vertical permeability, temperature, and salinity are relatively small compared to the above parameters. The vertical permeability controls the vertical exchanges between upper and lower layers, not the SWD with long injection intervals. Most perforations of the SWD wells are in the Bell Canyon Formation, followed by the Cherry Canyon Formation, and the least in the Brushy Canyon Formation. Perforated intervals (or open borehole completions) of most SWD wells in the DMG are not long enough to hydraulically connect all three formations (Fig. S16 and Fig. S17). This situation, combined with strong vertical anisotropy, translates into vertical differences in pressure buildups.

Results from the scenario with only oil production (and water injection) indicate that the producing process would, as expected, lower the pore pressure around production wells, and, in turn, affect the overall pore pressure increase in the DMG, even though the overall effects are small (differences in pressure buildups about 10–40 psi or 0.07–0.28 MPa) compared to the pressure buildup of only injection activities (100–400 psi or 0.7–2.8 MPa) (Fig. S15). The results from the scenario with both oil and water production (and water injection) show that the pressure buildup was reduced by 40–140 psi (0.28–0.97 MPa). This scenario represents a limit to low pressure buildup in which we assume that all the water produced from the DMG during the 2010–2020 decade (~1.5 billion barrels) were reinjected back into the DMG through the SWD wells. It is not part of the short cycle (production and reinjection for pressure maintenance) we hypothesized earlier for all DMG water production and ignored in the base case. The oil being produced is assumed to be water occupying the same pore volume. This is clearly a rough approximation as described in Hosseini and Nicot (2012).

The inclusion of the Capitan Reef in the model affects somewhat the pore pressure differentials at the edge of the DB (as much as 20 psi (0.14 MPa) at some points). However, its inclusion does not influence much the overall pressure evolution in the DMG because the main injection centers are away from the model boundaries.

6. Discussion

The model was calibrated avoiding overcalibration through individual well history matching, which would fit the data too closely and cannot reflect the overall necessary adjustments of the permeability field. It would also be a poor predictor of future pressure distribution. The model presents some limitations due to the lack of independent calibration data at dedicated monitoring wells, that is, time series of pressure data besides injection pressure history at injection wells. This, combined with the short correlation length of the permeability field (~3 miles or 3 gridblocks), increases the uncertainty of the pressure modeling results away from the injection centers. The somewhat pockmarked nature of the differential pressure maps (Fig. 4) emphasizes this lack of long-range pressure attenuation.

Another limitation is whether solution gas is released into the reservoir during production, which may also affect the pore pressure in the formations due to its large compressibility. Operationally however, operators are typically engaged in pressure maintenance early in production to avoid gas cap development, which would adversely impact oil production (Dutton et al., 2005). Therefore, we assume that the development of any small gas caps could be neglected in this regional model.

The model has other approximations. The model has no-flow boundary conditions, including the model top and bottom. The impact

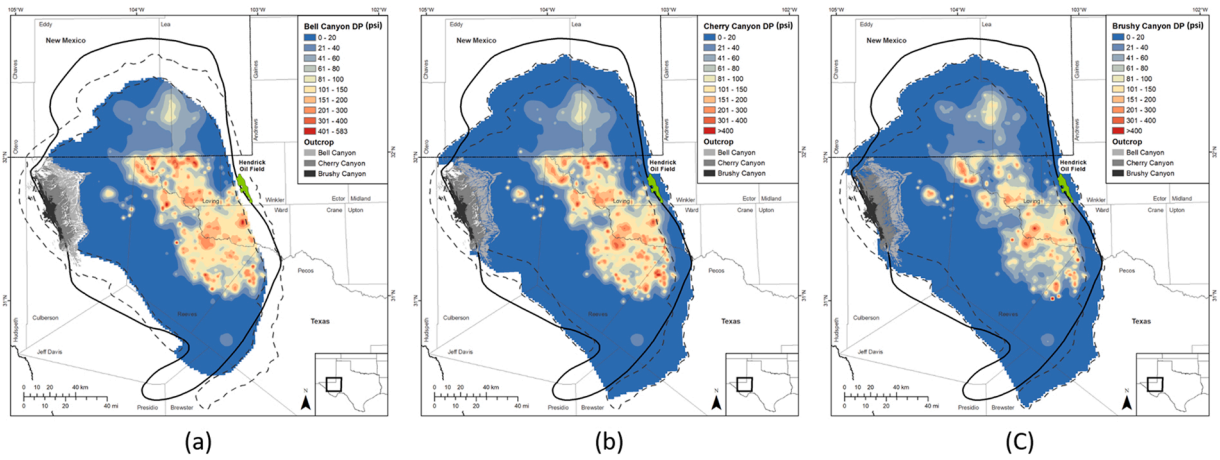

Fig. 4. Map of base case pressure increases in the three DMG formations: (a) Bell Canyon; (b) Cherry Canyon; and (c) Brushy Canyon.

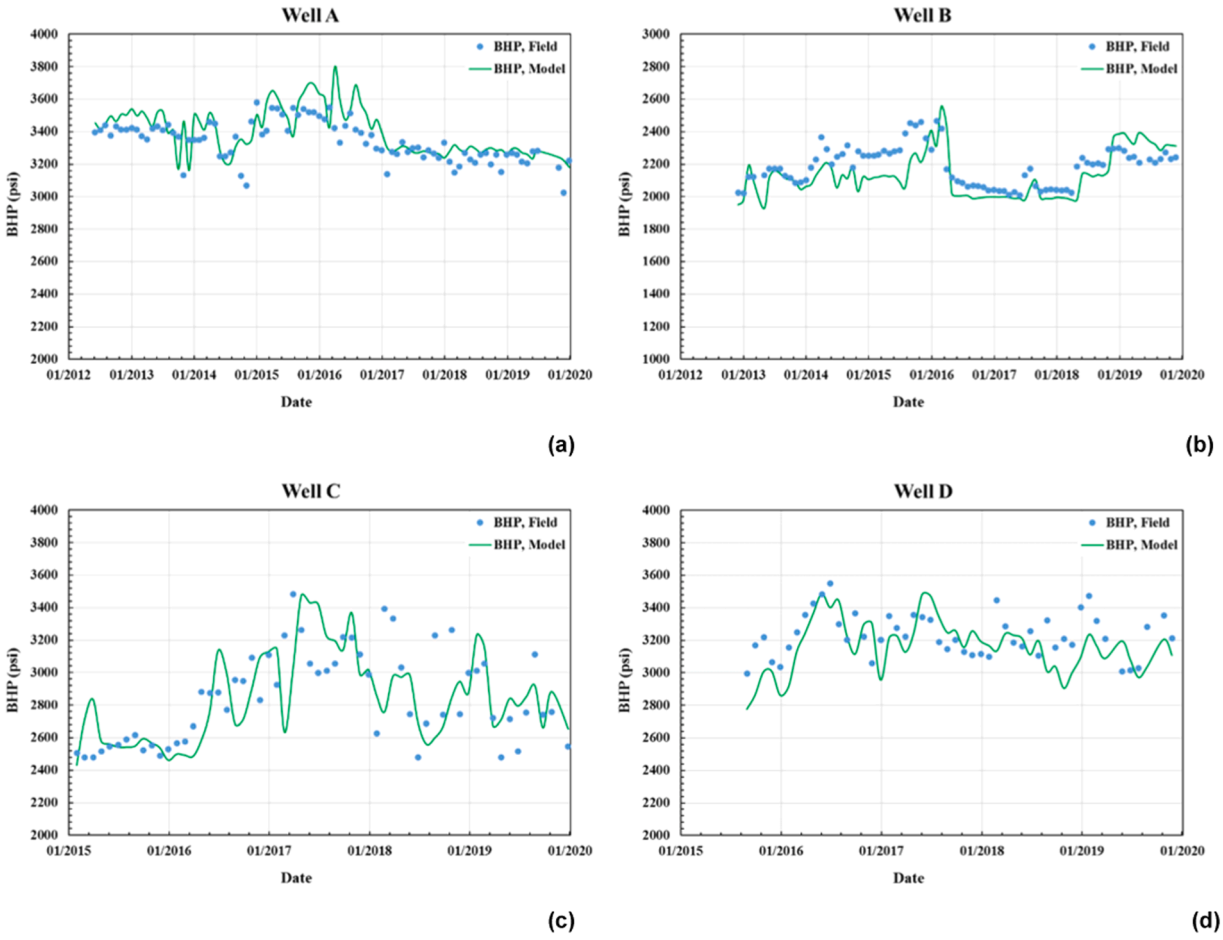

Fig. 5. Field (estimated from surface pressure) and modeled bottom-hole pressure time series at selected wells; (a) Well A is located in Eddy County, NM, and has a ~270 ft interval across the Bell Canyon and Cherry Canyon Formations; (b) Well B (Eddy County, NM), 1545 ft interval in the Cherry Canyon and Brushy Canyon Formations; (c) Well C (Loving County, TX), 1600 ft interval in the Bell Canyon and Cherry Canyon Formations; and (d) Well D (Loving County, TX), 2700 ft interval across the three DMG formations. 1000 psi is 6.9 MPa.

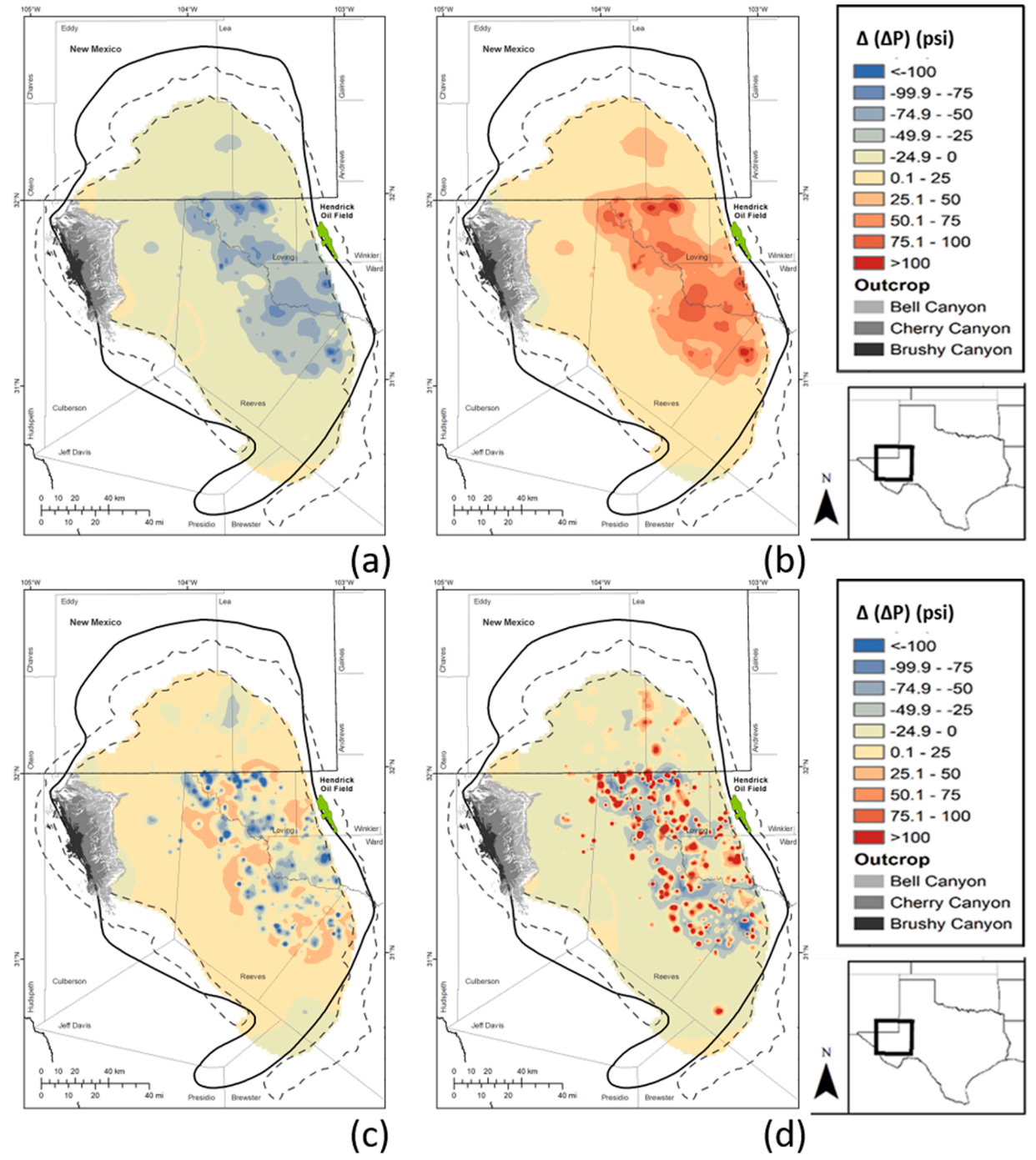

Fig. 6. Examples of sensitivity run results showing the impact of an (a) increased and (b) decreased pore compressibility by a factor of 2x and (c) increased and (d) decreased horizontal permeability by a factor of 5x. The maps show the difference between the pressure differentials of the base case and that of the sensitivity case (<0 pressure buildup difference means smaller pressure increase than in the base case). Pressure buildup difference is the difference between the pressure buildup of the sensitivity case and the base case.

of intense hydrocarbon and water production from the Wolfcamp and Bone Spring Formations, in particular from the Avalon Shale at the top of the Bone Spring reservoir in the northern sections of the DB (New Mexico) are unclear. A similar situation arose in the Fort Worth Basin of North Texas, with the producing Barnett Shale overlying the disposal interval (Ellenburger Group). A pair of studies gave rise to conflicting conclusions about impact of hydrocarbon production, or lack thereof (Gao et al., 2021; Chen et al., 2020). Compressibility of the adjacent formations could play a role in attenuating the pressure buildup, especially if gas occupies the pore

space. Factors such as oil compressibility, which is greater than water, have not been accounted for in models. The poor oil recovery of such systems, combined with the ~0.6 billion barrels of oil produced (surface conditions; ~1 billion barrels at reservoir conditions) suggests that at least twice that volume of oil remains in place. Such considerations are outside of the capabilities of a single phase flow model. Modeling to account for these subsurface conditions would require of the incorporation of two-phase flow parameters which currently are poorly constrained at the regional scale.

The rock units above and below the DMG could be affected by the SWD through dissolution or leakage along fractures and fault planes that impact the entire system and possibly enhances anisotropy of the horizontal permeability and reducing the vertical permeability. Operators have concluded that some Bone Spring - Avalon wells produce salt water that is injected into DMG SWD wells, similarly to what was observed between the Barnett Shale and the Ellenburger of the Fort Worth Basin (Gao et al., 2021).

The model results of pressure changes from 100 psi (0.7 MPa) to > 400 psi (>2.8 MPa) in some injection areas has brought attention to the possibility of induced seismicity along some existing faults in the study area. Although previous work (Peterie et al., 2018; Gao et al., 2021; Hennings et al., 2021a,2021b and 2021b) has shown that seismicity can be induced by pore pressure changes as low as 15 psi (0.1 MPa), the modeled regional pressure changes are higher than in many previously studied areas but consistent with the large amount of water injected in a short time span. Modeled pressure increase in the Fort Worth Basin reaches 200 psi (1.4 MPa) (Gao et al., 2021). In Oklahoma, pressure increases are described as < 200 psi (1.4 MPa) (Schoenball et al., 2018) despite a larger injection volume. However, the pressure increase is similar to but lower than that of another injection interval underlying the DMG footprint (Gao et al., 2020) where modeling suggests pressure increases > 400 psi (2.8 MPa) are not uncommon.

The alignment of the numerous small graben-bounding faults and regional maximum horizontal stress (S_{Hmax}) (Lund Snee and Zoback, 2017) suggests the faults are prone to reactivation, but also that fluid flow along the fault plane could be enhanced because of the increased permeability (Barton et al., 1995; Townend and Zoback, 2000; Hennings et al., 2012). The presence of faults is implicitly included in the injectivity-derived permeability values. Note that transverse permeability across faults, which could lead to pressure compartmentalization when low, has not been evaluated. Charzynski et al., 2019 suggested that the numerous normal faults serve as upward pathways for migrating fluid. This could lead to the dissolution of the overlying salt deposits, creating migration pathways and subsequent pore pressure attenuation in the DMG, a positive outcome that would nevertheless negatively affect the geotechnical stability of the impacted volumes. With the magnitudes and orientations of in-situ stresses within the faulted areas, the risk of reactivating existing faults from pore pressure variations can be evaluated by this work.

Nance (2020a) notes that the Castile Formation served as a barrier to the flow of hydrocarbon and guides hydrocarbon sourced from the DMG into CBP reservoirs. However, this barrier effect might be due to capillary and relative permeability effects rather than solely due to the low permeability of the Castile Formation. Nance (2020a) also posits that the lack of oil and gas accumulations west of the DB midline axis could be due to the absence of the Castile seal, suggesting that hydrocarbons are dissipated at the surface after migrating up the formation dip. This suggests less contrast in vertical and horizontal permeability values than assumed in this model.

If recent injection trends persist, additional salt water needs to be managed through SWD wells in DMG formations for the near future. Scanlon et al. (2020b) estimated that the volume of future produced water could be up to ~250 billion barrels during the productive life of the DB. The anticipated production suggests the need for efficient management of future SWD activities in the injection fields of DB with hazard mitigation in mind. With our estimation of the current pore pressure changes with SWD to-date, optimization of future injection patterns within allowable injection rates and pressures would be beneficial to SWD operators to effectively, and safely manage the finite SWD resource of the DMG.

7. Conclusions

A model of spatiotemporal evolution of pore pressure in the DMG of the DB can be very helpful to understand the initiation of seismic events, to assess possible fault reactivation and the causation of anomalous seismicity, and to develop estimations of the future hazards from induced seismicity and from regional pore pressure increase to manage the critical SWD resources of the region.

The modeling results indicate that:

- Pore pressure increases range from 100 to 400 psi (0.7–2.8 MPa), although they could be up to 500 psi (3.5 MPa), and higher locally, when in close proximity to SWD wells.
- Pressure increases are large enough to induce strong artesian behavior of potential conduits connecting land surface and DMG, and to sustain evaporite dissolution when initiated.
- Small pressure increases exist far away from the injection centers due to pressure diffusion.
- Pore pressure increases show high vertical variance due to the preferential injection into formations with better rock properties (i.e. Bell Canyon and Cherry Canyon Formations vs. Brushy Canyon Formation).
- The sensitivity analysis shows that pressure buildups are most sensitive to horizontal permeability and compressibility.
- Oil and related water production may limit pore pressure increase, especially around the production sites.
- Salinity of both formation water and injected water has a limited impact on pore pressure differentials.
- Presence of the Capitan Reef does relieve some pressure from the DMG, but it does not affect the increase in regional-scale pore pressure because it is located at the edge of the DB, away from most of the injection centers.

This work can be used for informing SWD management of the DMG. With increasing volumes of wastewater being injected into the target formations, effective and efficient control on the injection rates and patterns requires a thorough understanding of the pore pressure distributions and reservoir conditions.

CRediT authorship contribution statement

Jun Ge: Methodology, Investigation, Formal analysis, Validation, Writing – original draft. **J.-P. Nicot:** Conceptualization, Investigation, Writing – original draft preparation. **P.H. Hennings:** Project administration, Conceptualization, Supervision, Writing – review & editing. **K.M. Smye:** Formal analysis, Validation, Writing – review & editing. **S.A. Hosseini:** Software, Writing – review & editing. **R.S. Gao:** Software, Data curation, Writing – review & editing. **C.L. Breton:** Visualization.

Declaration of Competing Interest

The authors declare that they have no known competing financial interests or personal relationships that could have appeared to influence the work reported in this paper.

Acknowledgments

This work was supported by the Center for Integrated Seismicity Research (CISR) and its industrial affiliates at The University of Texas at Austin, Bureau of Economic Geology. We thank additional BEG contributors: Isabelle Pelletier, Robert C. Reedy, Elizabeth A. Horne, Kristine Uhlman, and Jana Robinson (creator of some graphics). We are also grateful to Railroad Commission of Texas staff, in particular Jim Moore, for helping us collect relevant well information. We also thank operators who shared details about their SWD operations. Finally, we thank IHS Markit for access to their Enerdeq database and Petra software, Computer Modelling Group (CMG) for access to their STARS and GEM softwares, and to Schlumberger for access to their Petrel software.

Appendix A. Supporting information

Supplementary data associated with this article can be found in the online version at doi:10.1016/j.ejrh.2022.101041.

References

AnonRuppel, S.C., ed., 2019, Anatomy of a Paleozoic Basin: The Permian Basin, USA (vol. 1): The University of Texas at Austin, Bureau of Economic Geology Report of Investigations 285; AAPG Memoir 118, 399 p., https://doi.org/10.23867/RI0285–1.

Barnes, C., Halihan, T., 2019. Patterns of seismicity associated with USGS identified areas of potentially induced seismicity. Groundwater 57, 86–96. https://doi.org/10.1111/gwat.12657.

Barton, C.A., Zoback, M.D., Moos, D., 1995. Fluid Flow. Potential. Act. faults Cryst. rock: *Geol.* v., 23, 8, pp. 683–686 doi: 10.1130/0091-7613(1995)023<0683:FFAPAF>2.3.CO;2.

Blondes, M.S., Gans, K.D., Engle, M.A., Kharaka, Y.K., Reidy, M.E., Saraswathula, V., Thordsen, J.J., Rowan, E.L., and Morrissey, E.A., *2018*, U.S. Geological Survey National Produced Waters Geochemical Database (ver. 2.3, January 2018): U.S. Geological Survey data release, https://doi.org/10.5066/F7J964W8.

Bloomfield, J.P., Lewis, M.A., Newell, A.J., Loveless, S.E., Stuart, M.E., 2020. Characterising variations in the salinity of deep groundwater systems: a case study from Great Britain (GB). J. Hydrol.: Reg. Stud. 28, 100684 https://doi.org/10.1016/j.ejrh.2020.100684.

Bourgoyne Jr., A.T., Millheim, K.K., Chenevert, M.E., Young Jr, F.S., 1986. Applied drilling engineering. SPE Textbook Series Vol. 2. Society of Petroleum Engineers, Richardson, Texas, United States.

Brown, A., 2019, Post-Permian history of the greater Permian Basin area, in Ruppel, S. C., ed., Anatomy of a Paleozoic basin: the Permian Basin, USA, vol. 1, ch. 5, The University of Texas at Austin, Bureau of Economic Geology Report of Investigations 285; AAPG Memoir 118, p.97–134, https://doi.org/10.23867/RI0285–1.

Bryndzia, L.T., Hows, A.M., Day-Stirrat, R.J., Nikitin, A., and Huvaz, O., 2019, Source(s) of Produced Water in the Permian Delaware Basin, West Texas: A Geochemical Analysis, Unconventional Resources Technology Conference, 23–25 July 2018, Houston, Texas. https://doi.org/10.105530/urtec-2019–102.

Carr, D.L., 2019, Stratigraphic Architecture of the Bone Spring Formation (Leonardian), Delaware Basin, New Mexico and Texas: An Interim Report, SPE/AAPG/SEG Unconventional Resources Technology Conference, Denver, Colorado, USA, July 2019, https://doi.org/10.15530/urtec-2019–645.

Cather, M., Gallegos, C., Chen, D., 2016. Accessing Produced Water Data in New Mexico: Improving and Updating the NM Produced Water Quality Database and Web Site N. Mex. Water Resour. Res. Inst. Tech. Complet. Rep. No., 375, p. 51.

Chen, R., Xue, X., Park, J., Datta-Gupta, A., King, M.J., 2020. New insights into the mechanisms of seismicity in the Azle area, North Texas. Geophysics 85, EN1–EN15. https://doi.org/10.1190/geo2018-0357.1.

Charzynski, K., Faith, K. Fenton, Z., Shedeed, A., McKee, M., Bjorlie, S., Richardson, M., 2019, Delaware basin horizontal Wolfcamp case study: mitigating H2S and excessive water production through isolating densely fractured intervals correlative to seismically mapped shallow graben features in the Delaware Mountain Group: Unconventional Resources Technology Conference, no.1037, Denver, CO, 22–24 July, 16 pp., https://doi.org/10.15530/urtec-2019–1037.

Computer Modeling Group (CMG), 2019, STARS User Guide. ⟨https://www.cmgl.ca/stars⟩.

Dutton, S.P., 2008. Calcite cement in Permian deep-water sandstones, Delaware Basin, West Texas: origin, distribution, and effect on reservoir properties. AAPG Bull. 92 (6), 765–787. https://doi.org/10.1306/01280807107.

Dutton, S.P., Barton, M.D., Malik, M.A., Asquith, G.B., Guzman, J.I., Clift, S.J., Cole, A.G., Casteel, J., 1998. Application of Advanced Reservoir Characterization, Simulation, and Production Optimization Strategies to Maximize Recovery in Slope and Basin Clastic Reservoirs, West Texas (Delaware Basin) (No. DE-FC22-95BC14936–17). National Petroleum Technology Office, Tulsa, OK (US).

Dutton, S.P., Flanders, W.A., Barton, M.D., 2003. Reservoir characterization of a Permian deep-water sandstone, East Ford field, Delaware basin, Texas. AAPG Bull. 87 (4), 609–627. https://doi.org/10.1306/10100201085.

Dutton, S.P., Kim, E.M., Broadhead, R.F., Raatz, W.D., Breton, C.L., Ruppel, S.C., Kerans, C., 2005. Play analysis and leading-edge oil-reservoir development methods in the Permian basin: increased recovery through advanced technologies. AAPG Bull. 89 (5), 553–576. https://doi.org/10.1306/12070404093.

Dvory, N.Z., Zoback, M.D., 2021. Prior oil and gas production can limit the occurrence of injection-induced seismicity: A case study in the Delaware Basin of western Texas and southeastern New Mexico, USA. Geology V (49). https://doi.org/10.1130/G49015.1.

EIA, 2020, Wolfcamp, Bone Spring, Delaware Shale Plays of the Delaware Basin, Permian Basin, Part I, Geology Review, U.S. Energy Information Administration, 38pp., ⟨https://www.eia.gov/maps/pdf/Permian-pI_Wolfcamp-Bonespring-Delaware.pdf⟩.

Ewing, J.E., V.A. Kelley, Toya L. Jones, T. Yan, A. Singh, Ph.D., D.W. Powers, R.M. Holt, J.M. Sharp, 2012, Final Groundwater Availability Model Report for the Rustler Aquifer, Texas Water Development Board contract report, variously paginated.

Ferguson, G., McIntosh, J.C., Grasby, S.E., Hendry, M.J., Jasechko, S., Lindsay, M.B.J., Luijendijk, E., 2018. The persistence of brines in sedimentary basins. Geophys. Res. Lett. 45, 4851–4858. https://doi.org/10.1029/2018GL078409.

Frohlich, C., Hayward, C., Rosenblit, J., Aiken, C., Hennings, P., Savvaidis, A., et al., 2020. Onset and cause of increased seismic activity near Pecos, West Texas, United States, from observations at the Lajitas TXAR seismic array. e2019JB017737 J. Geophys. Res.: Solid Earth 125. https://doi.org/10.1029/2019JB017737.

Galloway, W.E., Ewing, T.E., Garrett, C.M., Tyler, N., Bebout, D.G., 1983, Atlas of Major Texas Oil Reservoirs, The University of Texas at Austin Bureau of Economic Geology Special Publication Atlas # AT0002, 139pp.

Gao, R.S., Nicot, J.-P., Hennings, P.H., La Pointe, P., Smye, K.M., Horne, E.A., Dommisse, R., 2021. Low pressure build-up with large disposal volumes of oilfield water: a flow model of the Ellenburger Group, Fort-Worth Basin, North-Central Texas. AAPG Bull. https://doi.org/10.1306/03252120159.

Gao, S., Nicot, J.-P., Hennings, P., 2020, Preliminary hydrogeological modeling of produced water deep injection in the Delaware Basin for pore pressure characterization (abs.): Geological Society of America Abstracts with Programs, v. 52, no. 6, 1 p., http://doi.org/10.1130/abs/2020AM-358666.

Gogri, M.P., Rohleder, J.M., Kabir, C.S., Pranter, M.J., Reza, Z.A., 2018. Prognosis for safe water-disposal-well operations and practices that are based on reservoir flow modeling and real-time performance analysis. SPE Reserv. Eval. Eng. 21, 576–592. https://doi.org/10.2118/187083-PA.

Hall, H.N., 1953. Compressibility of reservoir rocks. J. Pet. Technol. 5 (01), 17–19. SPE–953309–G.

Hampton, B.D., 1989, Carbonate Sedimentology of the Manzanita Member of the Cherry Canyon Formation, in Subsurface and Outcrop Examination of the Capitan Shelf Margin, Northern Delaware Basin, P.M. Harris and G.A. Grover, Eds, https://doi.org/10.2110/cor.89.13.0431.

Healy, J.H., Rubey, W.W., Griggs, D.T., Raleigh, C.B., 1968. The Denver earthquakes. Science 161, 1301–1310. https://doi.org/10.1126/science.161.3848.1301.

Hennings, P., Allwardt, P., Paul, P., Zahm, C., Reid Jr., R., Alley, H., Kirschner, R., Lee, B., Hough, E., 2012. Relationship between fractures, fault zones, stress, and reservoir productivity in the Suban gas field, Sumatra, Indonesia. AAPG Bull. 96 (4), 753–772. https://doi.org/10.1306/08161109084.

Hennings, P.H., Lund Snee, J.E., Osmond, J., DeShon, H.R., Dommisse, R., Horne, E., Lemons, C., Zoback, M.D., 2019. Injection-induced seismicity and fault-slip potential in the Fort Worth Basin, Texas. Bull. Seismol. Soc. Am. 109 (5), 1615–1634. https://doi.org/10.1785/0120190017.

Hennings, P.H., Dvory, N., Horne, E.A., LI, P., Savvaidis, A., Zoback, M., 2021a. Stability of the fault systems that host induced earthquakes in the Delaware Basin of West Texas and Southeast New Mexico. Seism. Rec. https://doi.org/10.1785/0320210020.

Hennings, P.H., Nicot, J.P., Gao, R.S., DeShon, H.R., Lund Snee, J.-E., Morris, A.P., Brudzinski, M.R., Horne, E.A., Breton, C., 2021b. Pore pressure threshold and fault slip potential for induced earthquakes in the dallas-fort worth area of north central Texas. Geophys. Res. Lett. https://doi.org/10.1029/2021GL093564.

Hiss, W.L., 1976, Structure of the Permian Guadalupian Capitan aquifer, southeastern New Mexico and western Texas: U. S. Geological Survey Open-File Report 76–0053, 338 p.

Hiss, W.L., 1980. Mov. Ground Water Permian Guadalupian aquifer Syst., Southeast. N. Mex. West. Tex. Trans. -Pecos Reg. N. Mex. Geol. Soc., Guideb. 31st Field Conf., pp. 289–294.

Horne, E.A., Hennings, P.H., Zahm, C.K., 2021, Basement Structure of the Delaware Basin, in Callahan, O. A., Eichhubl, P., eds., The Geologic Basement of Texas: a volume in honor of Peter Flawn, Texas Bureau of Economic Geology Report of Investigations No. 286, https://doi.org/10.23867/RI0286C6.

Hosseini, S.A., Nicot, J.P., 2012. Numer. Model. a Multiph. Water-oil-CO2 Syst. Using a Water-CO2 Syst.: Appl. far Field a U. S. Gulf Coast Reserv.: *Int. J. Greenh. Gas. Control* v., 10, pp. 88–99 doi: 10.1016/j.ijggc.2012.06.001.

Hurd, G.S., Kerans, C., Frost, E.L., Simo, J.A., Janson, X., 2018. Sediment gravity-flow deposits and three-dimensional stratigraphic architectures of the linked Cutoff, upper Bone Spring, and upper Avalon system, Delaware Basin. AAPG Bull. 102 (9), 1703–1737. https://doi.org/10.1306/02061817121.

IHS, 2017–2020, IHS Enerdeq Browser download, ⟨https://penerdeq.ihsenergy.com/thin2/secure/about.jsf⟩.

Jones, I.C., 2014, Conceptual model: Capitan Reef Complex Aquifer: Texas Water Development Board, unpublished report, 174pp, ⟨https://www.twdb.texas.gov/groundwater/models/gam/crcx/crcx.asp⟩.

Kang, M., Ayars, J.E., Jackson, R.B., 2019. Deep groundwater quality in the southwestern United States. Environ. Res. Lett. 14, 034004 https://doi.org/10.1088/1748-9326/aae93c.

Kim, J.-W., Lu, Z., Kaufmann, J., 2019. Evolution of sinkholes over Wink, Texas, observed by high-resolution optical and SAR imagery. Remote Sens. Environ. 222, 119–132. https://doi.org/10.1016/j.rse.2018.12.028.

King, P.B., 1948, Geology of the southern Guadalupe Mountains, Texas (Vol. 215). US Government Printing Office.

Knowles, D.B., Lang, J.W., 1947. Preliminary Report on the Geology and Ground-Water Resources of Reeves County Texas Tex. Board Eng. Rep., M226, p. 87.

Langenbruch, C., Zoback, M.D., 2016. How will induced seismicity in Oklahoma respond to decreased saltwater injection rates? Sci. Adv. 2 (22), e1601542 https://doi.org/10.1126/sciadv.1601542.

Langevin, C.D., Guo, W., 2006. MODFLOW/MT3DMS-based simulation of variable-density ground water flow and transport. Groundwater 44, 339–351. https://doi.org/10.1111/j.1745-6584.2005.00156.x.

Lee, M.K., Williams, D.D., 2000. Paleohydrology of the Delaware basin, western Texas: overpressure development, hydrocarbon migration, and ore genesis. AAPG Bull. 84 (7), 961–974. https://doi.org/10.1306/A9673B80-1738-11D7-8645000102C1865D.

Lemons, C.R., Hennings, P.H., Dommisse, R., Nicot, J.-P. Smye, K., 2017, Protocols and common pitfalls in disposal data handling for induced seismicity geomodels (extended abstract), Unconventional Resources Technology Conference, Texas, 24–26 July 2017, https://doi.org/10.15530/URTEC-2017–2667788.

Lemons, C.R., McDaid, G., Smye, K.M., Acevedo, J.P., Hennings, P.H., Banerji, D.A., Scanlon, B.R., 2019. Spatiotemporal and stratigraphic trends in salt-water disposal practices of the Permian Basin, Texas and New Mexico, United States. Environ. Geosci. 26 (4), 107–124. https://doi.org/10.1306/eg.06201919002.

Lund Snee, J.E., Zoback, M.D., 2017. State Stress Permian Basin, Tex. N. Mex.: Implic. Induc. Seism.: *Lead. Edge* v., 37, 2, pp. 127–134 doi: 10.1190/tle37020127.1.

McNeal, R.P., 1965, Hydrodynamics of the Permian Basin, in Fluids in Subsurface Environments, A. Young and J.E. Galley Ed., *AAPG Memoir #4* , p.308–326, https://doi.org/10.1306/M4360C12.

Morris, A.P., Hennings, P.H., Horne, E.A., Smye, K.M., 2021. Stability of basement-rooted faults in the Delaware Basin of Texas and New Mexico, USA. J. Struct. Geol. 149, 104360 https://doi.org/10.1016/j.jsg.2021.104360.

Nance, H.S., 2020a, Upper Permian Delaware Mountain Group: Record of Highstand/Lowstand Platform Shedding, in Ruppel, S.C., ed., Anatomy of a Paleozoic basin: the Permian Basin, USA (chapter 24, v. 2): The University of Texas at Austin, Bureau of Economic Geology Report of Investigations 285; AAPG Memoir 118. https://doi.org/10.23867/RI0285–2.

Nance, H.S., 2020b, Guadalupian (Artesia Group) and Ochoan shelf successions of the Permian Basin: effects of deposition, diagenesis, and structure on reservoir development, in Ruppel, S.C., ed., Anatomy of a Paleozoic basin: the Permian Basin, USA (vol. 2, ch. 25): The University of Texas at Austin, Bureau of Economic Geology Report of Investigations 285; AAPG Memoir 118, p. 437–496. https://doi.org/10.23867/RI0285–2.

Newman, G.H., 1973. Pore-volume compressibility of consolidated, friable, and unconsolidated reservoir rocks under hydrostatic loading (Society of Petroleum Engineers). J. Pet. Technol. 25, 129–134. https://doi.org/10.2118/3835-PA.

Nicot, J.P., 2021, *Hydrogeology of the Texas Basement*, in Callahan, O.A., Eichhubl, P., eds., The Geologic Basement of Texas: a volume in honor of Peter Flawn. Texas Bureau of Economic Geology Bureau of Economic Geology Report of Investigations No. 286, https://doi.org/10.23867/RI0286C5.

Nicot, J.-P., Scanlon, B.R., 2012. Water use for shale-gas production in Texas. U.S. Environ. Sci. Technol. 46, 3580–3586. https://doi.org/10.1021/es204602t.

Nicot, J.-P., Huang, Y., Wolaver, B.D., Costley, R., 2013. Flow and salinity patterns in the low-transmissivity upper Paleozoic Aquifers of North-Central Texas. GCAGS J. 2, 53–67.

Nicot, J.-P., Scanlon, B.R., Reedy, R.C., Costley, R., 2014. Source and fate of hydraulic fracturing water in the Barnett Shale: a historical perspective. Environ. Sci. Technol. 48 (4), 2464–2471. https://doi.org/10.1021/es404050r.

Nicot, J.-P., Darvari, R., Eichhubl, P., Scanlon, B.R., Elliott, B.A., Bryndzia, L.T., Gale, J.F., Fall, A., 2020. Origin of low salinity, high volume produced waters in the Wolfcamp Shale (Permian), Delaware Basin, USA. Appl. Geochem. 122, 104771 https://doi.org/10.1016/j.apgeochem.2020.104771.

Ortiz, J.P., Person, M.A., Mozley, P.S., Evans, J.P., Bilek, S.L., 2019. The role of fault-zone architectural elements on pore pressure propagation and induced seismicity. Groundwater 57, 465–478. https://doi.org/10.1111/gwat.12818.

Paine, J.G., Buckley, S., Collins, E.W., Wilson, C.R., Kress, W., 2009, Assessing sinkhole potential at Wink and Daisetta using gravity and radar interferometry. In: Proceedings of the 22nd Symposium on the Application of Geophysics to Engineering and Environmental Problems, Fort Worth, Texas, March 29-April 2, p.480–488, https://doi.org/10.4133/1.3176733.

Peterie, S.L., Miller, R.D., Intfen, J.W., Gonzales, J.B., 2018. Earthq. Kans. Induc. Extrem. far-field Press. Diffus.: *Geophys. Res. Lett.* v. 45 , pp.1395–1401 doi: 10.1002/2017GL076334.

Potter, E.C., Walsh, M.P., Breton, C.L., Lemons, C., Reedy, R.C., 2020, Oil and gas production, Permian Basin: a giant conventional oil province being transformed by shale oil production, in Ruppel, S.C., ed., Anatomy of a Paleozoic basin: the Permian Basin, USA (vol. 2, ch. 26): The University of Texas at Austin, Bureau of Economic Geology Report of Investigations 285; *AAPG Memoir* 118, p. 497–526.

Rittenhouse, S., Li, Y., Hughston-Kennedy, K., Fritz, J., Pritchard, J., Cassel, L., Mooney, T., 2017, Delaware Basin Leonard Reservoir Characterization, New Mexico and Texas, Unconventional Resources Technology Conference, 24–26 July 2017, Austin, Texas, USA, https://doi.org/10.15530/URTEC-2017–2668602.

Robertson, W.M., Allen, J.T., Wolaver, B.D., Sharp, J.M., 2019. Arid land spring response to mesoscale precipitation: implications for groundwater-dependent ecosystem sustainability. J. Hydrol. Vol. 570, 850–862. https://doi.org/10.1016/j.jhydrol.2018.12.074.

Saini, D., Mezei, T., 2016. Potential use of water associated with conventional oil production and sea water as base fluids for hydraulic fracturing operations: effect of water chemistry on crosslinking and breaking behaviors of guar gum-based fracturing fluid formulations. Energy Environ. Res 6 (1), 31–43. https://doi.org/10.5539/eer.v6n1p31.

Savvaidis, A., Lomax, A., Breton, C., 2020. Induc. Seism. Del. Basin, West Tex., Is. caused Hydraul. Fract. Wastewater Dispos.: *Bull. Seismol. Soc. Am.*, 110, 5, pp. 2225–2241 doi: 10.1785/0120200087.

Scanlon, B.R., Reedy, R.C., Male, F., Walsh, M., 2017. Water issues related to transitioning from conventional to unconventional oil production in the permian basin. Environ. Sci. Technol. 51 (18), 10903–10912. https://doi.org/10.1021/acs.est.7b02185.

Scanlon, B.R., Reedy, R.C., Xu, P., Engle, M., Nicot, J.-P., Yoxtheimer, D., Yang, Q., Ikonnikova, S., 2020a. Can we beneficially reuse produced water from oil and gas extraction in the U.S.? Sci. Total Environ. 717, 137085 https://doi.org/10.1016/j.scitotenv.2020.137085.

Scanlon, B.R., Ikonnikova, S., Yang, Qi, Reedy, R.C., 2020b. Will water issues constrain oil and gas production in the United States? Environ. Sci. Technol. 54 (6), 3510–3519. https://doi.org/10.1021/acs.est.9b06390.

Schlumberger, 2019, information on Petrel software: ⟨https://www.software.slb.com/products/petrel⟩.

Schoenball, M., Walsh, F.R., Weingarten, M., Ellsworth, W.L., 2018. How faults wake up: The Guthrie-Langston, Oklahoma earthquakes. Lead. Edge 37 (2), 100–106. https://doi.org/10.1190/tle37020100.1.

Schultz, R., Skoumal, R.J., Brudzinski, M.R., Eaton, D., Baptie, B., Ellsworth, W., 2020. Hydraulic fracturing-induced seismicity. e2019RG000695 Rev. Geophys. 58. https://doi.org/10.1029/2019RG000695.

Sharp, J.M., Jr., 2001, *Regional groundwater flow systems in Trans-Pecos Texas*, in Mace, R.E., Mullican, W.F., III, and Angle, E.S., eds., Aquifers of West Texas: Texas Water Development Board, Austin, Texas, Report #R356, p. 41–55.

Sinclair, T.D., 2007. The Generation and Continued Existence of Overpressure in the Delaware Basin, Texas (Ph.D. these). Durham University, UK, p. 302 (Ph.D. these). ⟨http://etheses.dur.ac.uk/2289/⟩.

Skoumal, R.J., Brudzinski, M.R., Currie, B.S., 2018. Proximity of Precambrian basement affects the likelihood of induced seismicity in the Appalachian, Illinois, and Williston Basins, central and eastern United States. Geospheres 14 (3), 1365–1379. https://doi.org/10.1130/GES01542.1.

Skoumal, R.J., Barbour, A.J., Brudzinski, M.R., Langenkamp, T., Kaven, J.O., 2019. e2019JB018558Induc. Seism. Del. Basin, Tex.: *J. Geophys. Res. Solid Earth*, 125, 1. doi: 10.1029/2019JB018558.

Smye, K.D., Banerji, A., Eastwood, R., McDaid, G., Hennings, P., 2021. Lithology and reservoir properties of the Delaware Mountain Group of the Delaware Basin and implications for saltwater disposal and induced seismicity. J. Sediment. Res. 91 (11), 1113–1132. https://doi.org/10.2110/jsr.2020.134.

Standen, A., Finch, S., Williams, R., Lee-Brand, B. and Kirby, P., 2009. *Capitan reef complex structure and stratigraphy*. Prepared for the Texas Water Development Board, Austin, TX, 53pp., ⟨https://www.twdb.texas.gov/groundwater/models/gam/crcx/crcx.asp⟩.

Staniewicz, S., Chen, J., Lee, H., Olson, J., Savvaidis, A., Reedy, R., Breton, C., Rathje, E., Hennings, P., 2020. InSAR reveals complex surface deformation patterns over an 80,000 km2 oil-producing region in the Permian Basin. Geophys. Res. Lett. 47 (21) https://doi.org/10.1029/2020GL090151.

Townend, J., Zoback, M.D., 2000. How faulting keeps crust Strong.: *Geol.* v., 28, 5, pp. 399–402 doi: 10.1130/0091-7613(2000)28<399:HFKTCS>2.0.CO;2.

TWDB (Texas Water Development Board), 1972, A survey of the subsurface saline water of Texas, Vol.1, Report #157, prepared by Core Laboratories, Inc., Dallas, Texas, 113pp., ⟨http://www.twdb.texas.gov/publications/reports/numbered_reports/index.asp⟩.

Uliana, M.M., 2001, *The Geology and Hydrogeology of the Capitan Aquifer—A Brief Overview*, in Mace, R.E., Mullican, W.F., III, and Angle, E.S., eds., Aquifers of west Texas: Texas Water Development Board, Report 356, p. 153–166.

Uliana, M.M., Banner, J.L., Sharp Jr., J.M., 2007. Regional groundwater flow paths in Trans-Pecos, Texas inferred from oxygen, hydrogen and strontium isotopes. J. Hydrol. 334, 334–346. https://doi.org/10.1016/j.jhydrol.2006.10.015.

Van Der Loop, M., 2017, *Proposed stratigraphic Correlation framework, Wolfcamp of Delaware Basin, West Texas*, AAPG Division of Professional Affairs, Delaware Basin Playmaker's Forum, Midland, Texas, February 22, 2017, Search&Discovery # 90293, 25 slides.

Vidic, R.D., Brantley, S.L., Vandenbossche, J.M., Yoxtheimer, D., Abad, J.D., 2013. Impact of shale gas development on regional water quality. Science 340, 1235009. https://doi.org/10.1126/science.1235009.

West Texas Geological Society (WTGS), 1982, Selected Oil & Gas Fields in West Texas. a reprint of symposium vol. I, II, and III: Midland, Texas, Publication No. 82–75, 691p.

Zaengle, J.F., 1995. Teleogenetic controls on fluid flow, rock-water interaction and calcite cementation in Permian rocks of the Delaware basin, west Texas and southeast New Mexico. University of Michigan, p. 232 (Ph.D. dissertation).

Zhang, L., Wang, H., Li, Y., Pan, M., 2017. Quantitative characterization of sandstone amalgamation and its impact on reservoir connectivity. Pet. Explor. Dev. 44 (2), 226–233. https://doi.org/10.1016/S1876-3804(17)30025-3.